Published in final edited form as:
Future Oncol. 2009 September ; 5(7): 959–975. doi:10.2217/fon.09.77.

Diffusion-weighted imaging in head and neck cancers

Sanjeev Chawla,
Department of Radiology, University of Pennsylvania, B6 Blockley Hall, 423 Guardian Drive, Philadelphia, PA 19104, USA

Sungheon Kim,
Department of Radiology, University of Pennsylvania, B6 Blockley Hall, 423 Guardian Drive, Philadelphia, PA 19104, USA; and, Center for Biomedical Imaging, Department of Radiology, School of Medicine, New York University, New York, NY 10016, USA

Sumei Wang, and
Department of Radiology, University of Pennsylvania, B6 Blockley Hall, 423 Guardian Drive, Philadelphia, PA 19104, USA

Harish Poptani†
Department of Radiology, University of Pennsylvania, B6 Blockley Hall, 423 Guardian Drive, Philadelphia, PA 19104, USA, Tel.: +1 215 746 7387, Fax: +1 215 573 2113

Sanjeev Chawla: ; Sungheon Kim: ; Sumei Wang: ; Harish Poptani: poptanih@uphs.upenn.edu

Abstract

This article reviews the utility of diffusion-weighted imaging (DWI) in the diagnosis, prognosis and monitoring of treatment response in tumors arising in the head and neck region. The apparent diffusion coefficient (ADC) value, determined from DWI, can help in cancer staging and detection of subcentimeter nodal metastasis. The ADC value also discriminates carcinomas from lymphomas, benign lesions from malignant tumors and tumor necrosis from abscesses. Low pretreatment ADC values typically predict a favorable response to chemoradiation therapy. These promising reports indicate the potential of DWI as a potential biomarker for diagnosis and monitoring of treatment response in head and neck cancers. In view of the overlapping ADC values between different salivary gland tumors, care should be taken when interpreting these results and other imaging parameters should be considered for a better diagnosis. Susceptibility and motion-induced artifacts may sometimes degrade DWI image quality; however, novel techniques are being developed to overcome these drawbacks.

Keywords

apparent diffusion coefficient; diffusion-weighted imaging; head and neck cancers; lymphadenopathy; salivary gland tumors; squamous cell carcinomas of head and neck

Head and neck cancers account for the sixth most common type of cancer worldwide [1], with betel, tobacco and alcohol consumption being important risk factors causing significant

†Author for correspondence: Department of Radiology, University of Pennsylvania, B6 Blockley Hall, 423 Guardian Drive, Philadelphia, PA 19104, USA, Tel.: +1 215 746 7387, Fax: +1 215 573 2113, poptanih@uphs.upenn.edu.

Financial & competing interests disclosure
Grant support: NIH Grant RO1-CA102756 (HP). The authors have no other relevant affiliations or financial involvement with any organization or entity with a financial interest in or financial conflict with the subject matter or materials discussed in the manuscript apart from those disclosed.
No writing assistance was utilized in the production of this manuscript.

morbidity and mortality [2,3]. Squamous cell carcinoma (SCC) is the most common malignant histology in the head and neck region and originates from the epithelial lining of the upper aerodigestive tract [4,5]. These tumors are characterized by a multiphasic and multifactorial etiopathogenesis [6]. Approximately two-thirds of patients with head and neck cancers present with advanced stage disease, commonly involving regional lymph nodes, which require an amplified and aggressive treatment regimen consisting of neoadjuvant therapy and extensive surgery [7].

Numerous studies have demonstrated the potential of [^{18}F]-fluoro-2-deoxy-glucose (FDG) positron emission tomography (PET), alone [8,9] or in combination with computed tomography (CT) (hybrid PET/CT) [10], in evaluating SCC of the head and neck. However, lower spatial resolution and problems with discriminating neoplastic processes from inflammation and tissue reaction make the interpretation of PET images confounding, especially in the early post-radiation therapy phase [11]. Since FDG uptake is not specific to cancer, false positive findings, owing to inflammatory processes and metabolically active regions, are also common in the neck region [12].

Conventional MRI and CT continue to be the primary imaging modalities for evaluating head and neck cancers. However, both of these modalities rely on volumetric and morphological criteria and consequently suffer from low sensitivity and accuracy when making the diagnosis [13,14]. Moreover, post-treatment changes can be difficult to separate from tumor recurrence, as both entities may present with similar imaging features [15]. Advanced magnetic resonance techniques provide information regarding the metabolic, molecular and pathophysiological aspects of a tumor. These techniques include the use of proton [16,17] and phosphorous magnetic resonance spectroscopy [18,19], dynamic contrast-enhanced MRI (DCE-MRI) [20] and diffusion-weighted imaging (DWI) [21–28] in initial diagnostic characterization of head and neck cancers. Recently, DWI has also been proposed as a sensitive marker for monitoring treatment response in head and neck cancer [29]. The biophysical mechanism of DWI is based on the microscopic random translational motion of water molecules in biological tissues. The magnitude of this motion is characterized by its apparent diffusion coefficient (ADC) values. Brownian motion of water molecules is impeded by cellular packing, intracellular organelles, cell membranes and macromolecules present in various tissue compartments. Variation in ADC values reflects the alteration and redistribution of water molecules between intracellular and extracellular compartments of a tissue [30]. DWI has been investigated extensively in the evaluation of different brain pathologies [31,32]. In addition, it has also been applied to studies of the spinal cord and vertebral column [33], liver [34], kidneys and urinary tract [35].

In this review, the role of DWI in the characterization, prediction and monitoring of treatment response of head and neck cancers will be discussed. The basic principle, pathophysiologic mechanism and technical limitations in acquisition of DWI in the head and neck region will also be summarized along with potential ways to circumvent these limitations.

Basic principles of diffusion-weighted imaging

Physical basis of diffusion-weighted imaging

Diffusion-weighted images are typically acquired using strong magnetic field gradients to make the magnetic resonance signal sensitive to the molecular motion of water. In the presence of a magnetic field gradient, static spins accumulate phase shifts according to the equation:

$$\varphi(t)=\gamma B_0 t+\int G(t)\cdot x(t)dt.$$

The first term ($\gamma B_0 t$) in the equation represents the phase accumulation owing to the static magnetic field, while the second term:

$$\int G(t) \cdot x(t) dt,$$

reflects the effects of a magnetic field gradient. The phase accumulation owing to the gradient is proportional to the strength of the field gradient, spatial location of the spin and the duration of the gradient pulse.

Diffusion-weighted images are typically obtained by measuring the signal loss after the addition of a pair of rectangular diffusion sensitizing gradients (equal in strength and opposite in polarity and effect) to either side of the 180° pulse of a spin-echo (SE) sequence [36]. As a result of the first pulsed gradient, spins accumulate different phase shifts depending on their positions with respect to the gradient, while application of a second pulsed gradient, or 180° refocusing pulse, causes reversal of the phase shift. For stationary spins, the accumulated phase shift, as a result of the second gradient, will be similar in magnitude but opposite in polarity and therefore, the net phase shift will be zero at the time of echo, and the signal strength will remain intact. However, moving individual spins do not accumulate a similar phase shift during the two gradient pulses. Therefore, at the time of echo, phase shifts will be randomly distributed and will lead to signal attenuation on diffusion-weighted MRI. The degree of signal attenuation, after application of diffusion gradients, depends upon the duration and strength of the magnetic field gradients as well as the measurement of diffusivity and spin–spin relaxation time (T2) of mobile spins. The degree of signal loss can be represented by the term S/S_0, in which a signal after the application of diffusion gradients is represented by 'S', and a signal before the application of diffusion gradients by 'S_0'. The ratio of S/S_0 is proportional to the exponential of ADC (expressed as mm^2/s) and the degree of diffusion weighting (b; expressed as s/mm^2), and is represented by the equation: $S/S_0 = \exp(-b*ADC)$, as described by Stejskal and Tanner [36]. The signal intensity in each voxel is influenced by the choice of 'b' values, which depends upon the gradient amplitude, the time for which the diffusion gradients are applied and the time interval between diffusion gradients. The higher the b value, the more sensitive an image is to the effects of diffusion. In addition to b values, signal intensity also depends upon the echo time (TE) and the two parameters intrinsic to biological tissues – ADC and T2. However, if the TE values are kept constant, while varying the diffusion weighting on different DWI experiments, a pixel-by-pixel ADC map can be computed according the equation: $ADC = -(1/b)*[\log S/S_0]$.

Addition of diffusion-sensitizing gradients to the SE sequence generates a DWI image that reflects image contrast from both diffusion and T2 characteristics of the tissue. When measuring diffusion, long TEs are often required in order to achieve adequate diffusion-related signal attenuation, and therefore, DWI images are also heavily T2-weighted. As such, any hyperintensity in the DWI image may be attributed to either a reduction in ADC or to an increase in T2 values. The hyperintensity in DWI images owing to increased T2 is sometimes also referred to as 'T2 shine through'. In cystic lesions, where movement of water molecules is relatively free and the expected diffusivity is high (low signal intensity on DWI images), the T2 shine through effect leads to a high signal intensity on DWI images, owing to the longer T2 values of the unbound water. The ambiguous interpretation of such an image has revealed a number of pathologies that appear hyperintense on DWI images that mimic a stroke in the brain. Thus, DWI images should be used with caution in clinical interpretation [37]. A study by Colagrande *et al.* [37] suggests that the T2 shine through effect on DWI images can be reduced using large b values. On the other hand, generation of a pixel-by-pixel ADC map from DWI images, acquired with different b values, are more reliable for clinical interpretation than

DWI images alone, since these maps are not susceptible to the T2 shine through effect and provide true alterations in the diffusivity of a tissue [38,39].

Several diffusion imaging readout strategies are used to generate DWI images in clinical settings. These include fast spin echo (FSE) [40], single shot echo planar imaging (EPI) [41], segmented self-navigated FSE sequences (periodically rotated overlapping parallel lines with enhanced reconstruction [PROPELLER]) [42] and line scan DWI [28].

Biological basis of diffusion-weighted imaging

Self diffusion of water molecules is characterized as Brownian motion. When water molecules are unconstrained, the direction of motion of a given molecule is random. In biological tissue, the cell membrane and organelles form physical boundaries and provide barriers to the movement of water. The diffusion distance increases proportionally to the square root of diffusion time in a 3D space according to the Einstein equation: $<r^2> = 6Dt$. Thus, the effective diffusion distance for a water molecule is smaller in tissues than in bulk water, where the movement of water molecules is not impeded by any boundaries. As a consequence, the diffusion coefficient measured *in vivo* by DWI is always lower than that of free water and is hence termed ADC.

Biological tissue can be considered as a combination of intra- and extra-cellular compartments in which the water molecule is in a state of continuous exchange between these two compartments. Therefore, the observed signal attenuation in the diffusion experiment depends on the rate of exchange and the diffusion time. In the limit of slow exchange, water spins remain within their respective compartments during the diffusion time and signal attenuation follows a bi-exponential pattern. This bi-exponential behavior is explained by the equation: $S = S_0[f_1 \exp(-b_1ADC_1) + f_2 \exp(-b_2ADC_2)]$, where f_1 and f_2 are the volume fractions of water spins within each of the two compartments and $f_1 + f_2 = 1$; ADC_1 and ADC_2 are the ADCs in the two compartments. On the other hand, in the limit of fast exchange with complete redistribution of water between the two compartments during the diffusion time, the signal attenuation follows a single exponential behavior given by the equation: $S/S_0 = \exp(-b*ADC)$. The observed ADC for a two-compartment system includes contributions from both the intra-and extra-cellular environments and is approximated by the equation: $ADC = f_1ADC_1 + f_2ADC_2$. In most clinical DWI studies, the bi-exponential behavior of signal attenuation is not observed due to the low b-values used. Therefore, it is common practice to fit the DWI data to a single exponential decay model.

Diffusion-weighted imaging in characterization of head & neck tumors

A differential diagnosis of benign and malignant lesions of the head and neck is critical as it enables clinicians to implement appropriate management strategies for malignant lesions. Several promising studies have suggested the usefulness of DWI in the characterization of head and neck tumors [21–23,28]. In a study that included carcinomas, lymphomas, benign salivary gland adenomas and benign cysts, Wang *et al.* [21] reported that the mean ADC value of benign solid lesions was significantly higher than that of malignant tumors. In this study, lymphomas were reported to have significantly lower ADC values than carcinomas, which in turn, had significantly lower ADC values than benign solid tumors. A threshold ADC value of 1.22×10^{-3} mm^2/s provided an accuracy of 86%, sensitivity of 84% and specificity of 91% for predicting malignancy. These results were supported by Maeda *et al.* [28], who reported significantly lower ADC values in lymphomas compared with SCC of the head and neck. Representative magnetic resonance images from a patient with SCC of the head and neck is shown in Figure 1. These previous studies were performed using a 1.5 tesla (T) magnetic resonance system. However, a recent study demonstrated that DWI in head and neck cancers can also be performed at a higher magnetic field without degradation of the image quality due

to susceptibility artefacts, which are commonly observed at higher field strengths of 3T [23]. The authors in this study reported a significant difference in mean ADC values between benign ($1.50 \pm 0.48 \times 10^{-3}$ mm^2/s) and malignant ($1.07 \pm 0.29 \times 10^{-3}$ mm^2/s) lesions. While significant differences were observed in ADC values between SCCs and lymphomas and between benign and malignant tumors, there was some overlap in ADC values between these tumor types and thus, care should be taken when ADC values are used in isolation.

Some investigators have also reported significantly lower (restricted) ADC values in SCCs than in nontumoral soft tissues such as paraspinal musculature and the base of the tongue [43,44]. An inverse correlation has been observed between the ADC and cell density in brain tumors in humans [45,46], as well as in human melanoma xenografts transplanted in animal tumor models [47], suggesting that higher cellularity is generally associated with more restricted diffusion (low ADC values). A number of studies have discussed the possible causes of restricted diffusion in high-grade gliomas [48], brain lymphomas [49] and brain abscesses [50]. These lower ADC values have been attributed to the histopathological characteristics of malignant tumors such as an enlarged nuclear:cytoplasmic ratio, hyper-chromatism and hypercellularity [51]. The synergetic effect of these characteristics reduces the ratio of extracellular:intracellular volume and the diffusion space for water molecules, with a resultant decrease in ADC values. It has also been reported that ADC values of highly or moderately differentiated SCCs are higher than those of poorly differentiated SCCs [21,22]. The authors of these studies ascribed this finding to the presence of a more abundant macromolecular protein contents along with hypercellularity and a higher nuclear:cytoplasmic ratio associated with poorly differentiated SCC and the presence of a high degree of small foci of liquefactive necrosis in well-differentiated SCC, which was confirmed histopathologically.

Although these earlier studies demonstrated the potential of ADC in the characterization of head and neck cancers, they suffer from the small number of patients studied, as well as a certain degree of overlap between different tumor types. Image artefacts are also observed in DWI of the head and neck region because of continuous physiological motion from breathing and swallowing, as well as susceptibility-induced artefacts associated with a single shot EPI sequence. Therefore, care should be taken when translating the results of these published studies in routine clinical practice. Future multi-center studies in a large cohort of patients with identical imaging protocols are required to substantiate these promising preliminary results. As ADC maps suffer from relatively poor resolution, delineation of the tumor is typically performed on T2 or postcontrast spin-lattice relaxation (T1)-weighted images and the region of interest is then overlaid on ADC maps. Thus, DWI data should always be used in combination with other MRI sequences in evaluating head and neck cancers.

Diffusion-weighted imaging in cervical lymph nodes

The standard work-up for patients with SCC of the head and neck includes evaluation of pathological lymph nodes along with staging of the primary tumor and evaluation of the presence of distant metastasis before making a decision regarding the appropriate treatment regimen (chemoradiation therapy versus surgery), as lymphatic metastasis is an important mechanism of tumor spread [52]. The presence of lymphatic adenopathies in the neck largely determines the likelihood of locoregional control and the risk of distant metastasis. However, because of the location and complex tissue structures, clinical evaluation of metastatic neck lymph nodes is not very accurate. FDG-PET scans or conventional cross sectional MRI cannot reliably detect small tumor deposits within nonenlarged lymph nodes. It is also difficult to differentiate large inflammatory lymph nodes from metastatic lymphadenopathy [53]. It has been demonstrated that iron oxide particles, when injected intravenously, can gain access to lymph nodes by means of interstitial lymphatic fluid transport. Being paramagnetic, these agents induce a negative contrast on T2-weighted images in the presence of magnetic field

inhomogeneities (T2*). The metastatic lymph nodes accumulate the iron oxide particles and thus, appear hypointense on MRI images, while normal lymph nodes clear the iron oxide particles owing to efficient lymphatic drainage. Using this mechanism, smaller lymph-node metastases have been detected and the technique has also been used to distinguish benign from malignant lymph nodes in patients with head and neck cancers [54,55]. However, the use of additional intravenous injection (besides Gd-DTPA for diagnosis) and safety concerns regarding contrast-agent clearance have limited the use of iron oxide particles in the clinical settings.

Metastatic SCC lymph nodes are heterogeneous in nature and contain variable degrees of necrotic parts and keratin protein contents [56,57]. Based on these features, it can be hypothesized that these nodes are associated with alterations in water diffusivity and thus, DWI may play an important role in their characterization. In line with this hypothesis, several studies have reported the ability of DWI to discriminate malignant from benign lymph nodes in the neck [21,58], with the metastatic nodes exhibiting lower ADC values compared with benign lymph nodes. However, one DWI study reported significantly higher ADC values in metastatic lymph nodes than in benign lymphadenopathy [22]. The higher ADC of metastatic nodes may be explained by the presence of a large number of necrotic regions within the metastatic nodes in this study [22].

While detection of larger lymph nodes is possible by cross-sectional imaging with CT, MRI or PET scans, detection and assessment of subcentimeter (<10 mm) adenopathies remains a challenge, owing to the lower sensitivity and spatial resolution of these techniques. However, DWI has been demonstrated to have improved sensitivity in the detection of subcentimeter nodal metastases. In a recent study [25], DWI was reported to have a sensitivity of 76% and a specificity of 94% in the detection of 4–9 mm lymph nodes compared with the conventionally used turbo SE (TSE) MRI sequence, which only had a sensitivity of 7% and a specificity of 99.5% for detection of these lesions. The value of DWI in nodal staging was also investigated in this study, in comparison to histopathological staging, and the authors reported that DWI was superior to T2-weighted TSE imaging in accurate nodal staging. With a threshold ADC value of 0.94×10^{-3} mm^2/s, a sensitivity of 84%, specificity of 94% and accuracy of 91% was achieved in the differentiation of malignant from benign lymph nodes (Figure 2) [25]. In another study [53], the utility of DWI in characterization of small and nonpalpable cervical lymphadenopathy was studied. In this study, an ADC threshold value of 1.0×10^{-3} mm^2/s led to a high sensitivity of 92.3% and specificity of 83.9% in discriminating malignant from benign cervical lymph nodes. Furthermore, use of ADC values in combination with the other MRI parameters, such as size, border irregularity and degree of homogeneity for signal intensity on fat-suppressed T2-weighted images, significantly improved the discriminatory power of DWI in differentiating between benign and malignant nodes. In spite of the promising potential of ADC in detecting smaller nodes, the lower in-plane resolution of ADC maps and potential image artefacts, especially if nodes are located at the air–tissue interface, raise questions regarding the specificity and reproducibility of these results. Partial volume effects from the regions of interest used to measure ADC values of these small lymph nodes may also lead to inaccurate ADC values. Therefore, it is important to perform these studies in a larger patient population and across multiple sites in order to substantiate the role of DWI as a reliable method in detecting smaller nodes.

Diffusion-weighted imaging has also been used for the characterization of enlarged necrotic nodes that are associated with inflammation or neoplastic diseases, especially when differentiation between central necrosis of the metastatic nodes and infectious necrotic nodes is difficult using conventional MRI. Koc *et al.* [59] reported that abscesses and necrotic lymphadenitis appear hyperintense on DWI and exhibit lower ADC values compared with necrotic nodal metastases that appeared hypo-intense on DWI and resulted in higher ADC

values. These results are not surprising since it was previously reported that a higher protein component in infective lesions increases the viscosity and reduces water proton mobility leading to lower ADC values [50].

Diffusion-weighted imaging in differentiation between the viable & necrotic parts of malignant tumors

In the assessment of patients with cervical lymph nodes, fine needle aspiration cytology (FNAC) and/or an open biopsy is often performed to confirm or refute the diagnosis of a head and neck malignancy [60–62]. It has been recognized that the tiny amount of tissue obtained by biopsy may not be sufficient for a correct diagnosis and may lead to erroneous interpretation [63]. Therefore, delineation of viable and necrotic parts of a tumor is essential for determining the biopsy site and for diagnosis and treatment planning. The use of contrast-enhanced MRI is limited in stratifying tumor heterogeneity since these images typically demonstrate an overlap between viable and necrotic regions. While the enhanced part usually contains viable tumor cells, the non-enhanced part may contain both viable and necrotic cells. Using DWI, Razek *et al.* [27] reported an accurate delineation between the viable parts and necrotic regions of the tumor. The mean ADC value of viable tumors was reported to be significantly lower than that for necrotic parts in this study. The differentiation between viable and necrotic parts can be explained by the fact that water molecules within intact cell membranes of viable tumor cells are characterized by a relatively small mean free-path length, which results in restricted diffusion and low ADC values. On the other hand, tumor necrosis is characterized by increased membrane permeability and breakdown of the cell membrane, resulting in free diffusion and an increase in the mean free-path length of diffusing molecules. These changes result in decreased restriction and thereby increased diffusion of water molecules in the necrotic regions. These results suggest that DWI can assist in a better choice of site for tumor biopsy, which might ultimately decrease false-negative results and reduce the need for rebiopsy.

Diffusion-weighted imaging in differentiation between recurrent/residual tumors & post-treatment changes

Management of head and neck cancer involves multidisciplinary approaches that include surgery and chemoradiotherapy. Several factors impact the quality of life and survival of a patient, such as the nature, size and degree of infiltration of the primary tumor, nodal staging and the presence or absence of distant metastatic nodes. Other factors that may impart social and functional losses (such as impaired swallowing and eating, and speech deficit), as well as cosmetic deformity that may result from surgery, are also carefully weighed before making a final decision. Recently, novel treatment modalities such as induction chemotherapy and molecular targeted immunotherapy have also demonstrated significant improvements in clinical outcomes. A majority of the patients who develop advanced tumors are treated with induction chemotherapy, and concurrent chemo-radiotherapy with surgery usually reserved for salvage procedure [64–66]. Effects of radiation therapy include edema in the acute phase and a fibrous-inflammatory reaction, with formation of scar tissue in the adjacent normal soft tissues in the chronic phase. Postradiation changes may also cause thickening of soft tissue of the pharynx and larynx that may lead to difficulty in breathing and stridor [67]. Postirradiation biopsies, performed for diagnosis of residual/recurrent disease, are frequently equivocal [68, 69]. Surgeons are often reluctant to obtain multiple or deep biopsy specimens in previously irradiated areas for fear of initiating or aggravating radio-necrosis [70]. Despite aggressive and combined therapeutic regimes, tumors generally recur at, or near, the site of initial mass. Therefore, continuous surveillance of these patients after radiation therapy is crucial, since almost two-thirds of patients with head and neck cancer die prematurely, owing to delayed diagnosis and inadequate treatment of the recurrent tumor [71]. The distinction of irradiation

effects from recurrent tumors poses a common diagnostic dilemma for diagnostic CT and MRI, since both abnormalities exhibit similar imaging characteristics [15]. Although FDG-PET/CT holds promise in the detection of recurrent SCC of the head and neck [72], it leads to more false positives owing to inflammatory changes within the first 4 months after radiation therapy [12].

Diffusion-weighted imaging holds promise for distinguishing recurrent/residual tumors from radiation-induced changes (Figure 3) as it has been reported that ADC values can accurately differentiate persistent or recurrent tumors from nontumoral tissue, both in the early (<4 months) as well as the late (>4 months) postradiation therapy period [24]. The ADC maps exhibit a high sensitivity (94.6%), specificity (95.9%) and accuracy (95.5%) in the discrimination of tumoral and nontumoral tissues. Furthermore, when compared with CT or PET, DWI yielded fewer false positives, both in persistent primary sites and in persistent adenopathies [24]. In another study, areas of low DWI signal intensity and significantly lower ADC values from residual or recurrent tumors were observed in comparison to post-treatment changes that demonstrated areas of high signal intensity on ADC maps [26].

The differences in ADC values between recurrent tumors and radiation changes reflect the distinct differences between the histopathologic features and distribution of water molecules in tumors and radiation therapy-related changes. Malignant viable tumors have enlarged nuclei, hyperchromatism and generally exhibit hypercellularity. These histologic features lead to a reduction in the diffusion space of water protons in both the extra- and intra-cellular compartments, with a resultant decrease in ADC [73]. On the other hand, tissues with post-treatment changes have relatively low cellularity and increased interstitial space, associated with variable degrees of edema and inflammatory reaction or submucosal fibrosis, which results in an increase of the interstitial water content with fewer barriers for diffusion and a subsequent increase in the ADC values [74]. However, it is important to note that DWI might not always be sensitive in detecting early structural changes caused by radiation-induced injury. In a recent study, Philippens *et al.* [75] reported that ADC values were less sensitive than T2 values in detecting radiation damage of the gray matter of the spinal cord in rats. In a recently published provocative commentary by Hackney [76], it was suggested that the more readily available T2 imaging should be used in assessing radiation-induced injury in the spinal cord instead of diffusion imaging. While there may be some validity to these reports in the analysis of spinal cord injuries, further studies of SCC of the head and neck are necessary to establish the role of diffusion imaging in the differentiation of recurrent/residual tumors from radiation-induced injury.

Diffusion-weighted imaging in prediction & monitoring early treatment response

Concurrent chemotherapy along with intensity-modulated radiotherapy (IMRT) is widely used in the treatment of unresectable metastatic lymph nodes in SCC of the head and neck [64]. Despite many technological advances in surgery and aggressive therapeutic regimens, prognosis and clinical outcome of patients with SCC of the head and neck remain poor [77]. A reliable prediction of the tumor response based on assessment of the tumor microenvironment may assist in better selection of therapeutic strategies. Accurate prediction of treatment response or presence of nonresponsive tumors (using conventional approaches) can be critical in disease management since the optimal time window for successful treatment tailoring may be limited [78]. Therefore, reliable and reproducible imaging markers that can predict patients who are at a greater risk of progression of disease before commencement of treatment are needed. In addition, imaging markers that can assess therapeutic response at an early stage of treatment may assist in altering treatment regimens and help in improving the overall clinical outcome. Preclinical studies in brain tumor models have demonstrated the

sensitivity of DWI in detecting early changes induced by chemotherapy [79] or retrovirus-mediated gene therapy [80]. Lemaire *et al.* [81] reported that initial low ADC predicted tumor sensitivity to fluorouracil treatment in rat mammary tumors. Clinical DWI studies in brain [82] and rectal tumors [83] have reported that tumors with higher ADC values were associated with reduced response to therapy. Pretreatment ADC values have also been used to separate complete responders from partial responders in patients with cervical cancers undergoing chemoradiation therapy [84]. The results of these studies are consistent with the hypothesis that a high ADC value may be indicative of the presence of micronecrosis and consequently, a greater resistance to treatment.

We recently reported the potential of ADC in the prediction and early detection of response to chemoradiation therapy in SCCs of the head and neck (Figure 4) [29]. We observed that the pretreatment mean ADC value of complete responders ($1.04 \pm 0.19 \times 10^{-3}$ mm^2/s) was significantly lower than that of patients who exhibited a partial or no response ($1.35 \pm 0.30 \times 10^{-3}$ mm^2/s). A significant increase in ADC within 1 week of treatment was also observed in complete responders and this remained high until the end of treatment (Figure 5). The change in ADC values from pre-treatment to after 1 week of therapy resulted in a sensitivity of 86% and specificity of 83%, indicating the potential of ADC in monitoring early treatment response in SCCs of the head and neck.

Elevated tumor perfusion parameters (blood flow, blood volume and vascular permeability), secondary to tumor neovascularity, have been reported in head and neck cancers using contrast-enhanced dynamic CT [85], arterial spin labeling [86], blood oxygen level dependent (BOLD) MRI [87] and dynamic contrast-enhanced perfusion-weighted imaging [20]. While tumor vasculature plays a critical role in supplying nutrients and oxygen to tumor cells, it also provides a means for effective delivery of chemotherapeutic agents to the tumors. It has been reported that SCC patients with higher pretreatment blood flow/blood volume values respond more positively to therapy than patients with a lower blood flow/volume [88–90]. Cytotoxic chemotherapy triggers apoptotic pathways leading to reduced cell density and enlarged extra-cellular space [91], which might lead to a higher ADC of the tumor after treatment. It is plausible that tumors with higher blood supplies will have elevated oxygenation and accessibility to cytotoxic drugs, resulting in increased apoptotic and/or necrotic regions within the tumor following chemotherapy. This phenomenon might explain the increased ADC values observed in complete responders compared with partial or nonresponders, as reported by Kim *et al.* [29].

Diffusion-weighted imaging in salivary gland tumors

Salivary gland tumors are relatively uncommon and represent less than 3% of all head and neck cancers. Among all glands, the parotid glands offer the largest variety of histological types of neoplasm. Preoperative diagnosis of parotid gland tumors is crucial, since a more aggressive approach to treat malignant tumors is preferred in order to reduce further complications. Even between benign lesions, it is important to determine the exact histological subtypes as the treatment plan differs depending on whether the tumor is a pleomorphic adenoma or a Warthin tumor. Superficial parotidectomy with preservation of the facial nerve, or partial superficial parotidectomy with removal of the tumor capsule, is recommended for patients with pleomorphic adenoma, whereas enucleation or superficial parotidectomy with preservation of the facial nerve is adapted for patients with a Warthin tumor [92,93]. While the risk of local recurrence of Warthin tumors is approximately 2%, the risk for local recurrence of pleomorphic adenomas is reported to be approximately 85% [92,93]. FNAC is generally used in the preoperative diagnosis of salivary gland masses. However, the results of FNAC are not always conclusive owing to insufficient sample size of the specimen or because of the deep location of the tumor. In addition, tumor spread as a result of FNAC is a subject of controversy, with

some authors raising concerns that FNAC is potentially associated with spillage of tumor cells into the vascular compartments, which can lead to local recurrence, especially in pleomorphic adenomas and malignant lesions [94,95]. On the other hand, some reports suggest that the mere presence of tumor-cell deposits along the needle tract after FNAC administration might not necessarily indicate spread of a viable tumor [96]. Furthermore, it has been reported that FNAC of salivary gland masses by smaller gauge needles is a safe and reliable procedure [97].

Diagnostic cross-sectional MRI has limited utility in the differentiation of salivary gland tumors [98,99]. However, DWI has been demonstrated to have potential in determining different histological subtypes of salivary gland tumors [100–102]. Habermann *et al*. reported significantly different ADC values in pleomorphic adenomas, Warthin tumors and mucoepidermoid carcinomas [100]. A recent study demonstrated that pleomorphic adenomas were distinguishable from all other entities on the basis of ADC values, with the exception of myoepithelial adenomas [103]. However, there may be some instances with considerable overlap between these tumor types and ADC values alone may not be enough to differentiate benign from malignant salivary gland tumors [104]. It has also been reported that combining DWI with DCE-MRI could improve the diagnostic accuracy of parotid gland tumors [102]. Histopathologically, pleomorphic adenomas contain epithelial, myoepithelial and stromal cellular components. Most of the epithelial components of glandular nature and adenomatous tumors can contain areas of accumulated fluid [105]. Both can contribute to the high ADC values, as has been observed in pleomorphic adenomas. By contrast, Warthin tumors consist of abundant lymphoid tissues that include polyclonal lymphocytes with conspicuous follicles and germinal centers. These components may be responsible for the low ADC values observed in Warthin tumors [100,103].

Influence of field strength on apparent diffusion coefficient values

The advent of commercially available 3T magnetic resonance systems, along with dedicated phase array coils and parallel imaging techniques, enable better quality DWI images and ADC maps with a substantially improved signal:noise ratio, compared with those acquired with the 1.5T magnetic resonance system. Since most DWI studies on head and neck cancers have been published on 1.5T, it is unclear as to whether these results can be translated to the 3T field strength. While significant differences in ADC values from the gray and white matter regions of the brain have been reported between 1.5T and 3T field strengths [106], no such studies have been performed in head and neck cancers. In a small cohort, we performed DWI on the neck region of three healthy human subjects at both 1.5 and 3T scanners within 1 h and observed no difference in ADC values from the submandibular glands when measured using either magnet [29]. Using a threshold ADC value of 1.3×10^{-3} mm^2/s from a 3T magnet, Srinivasan *et al.* [23] reported differentiation of benign from malignant head and neck cancers. It should be noted that this threshold value was similar to that reported earlier (1.22×10^{-3} mm^2/s) at a 1.5T field by Wang *et al.* [21]. These reports indicate that ADC is a field strength-independent parameter and thus, can be used to compare results across different sites and field strengths. However, more DWI studies comparing the ADC values at different field strengths from the head and neck regions are warranted.

Technical limitations of diffusion-weighted imaging in the head & neck region

While the above-mentioned studies clearly demonstrate the potential of DWI in the diagnosis, prognosis and monitoring of treatment response in tumors of the head and neck, there are a few limitations in performing DWI of the head and neck region that need to be kept in mind when proposing DWI as a potential biomarker for tumors arising in the head and neck. The inherent drawbacks associated with EPI, such as susceptibility artefacts, chemical shift artefacts and Nyquist (N/2) ghosting artefacts in the phase-encoding direction, are much more

severe in the neck region. In the Nyquist (N/2) artefact, image ghosts appear in half the field of view in the phase-encoding directions. These artefacts arise as a result of a zigzag data acquisition pattern in EPI sequence, in which the signal is sampled during both the positive and negative half of the frequency-encoding gradient. If the echoes are acquired slightly off-center, the even and odd lines of the k-space become staggered. Since the even and odd echoes sample N/2 data points (half the Nyquist rate of sampling), the artefact is seen as a ghost image shifted by N/2 pixels. This artefact can be reduced by using a calibrated scan obtained at the beginning of the EPI sequence with the phase-encoding gradient turned off [107].

Susceptibility artefacts result from the various air spaces within the head and neck region, including sino–nasal spaces, mastoid air cells and aerodigestive tracts. Furthermore, dental fillings with metallic materials may increase the occurrence of susceptibility artefacts on images in the head and neck. Consequently, it becomes difficult to identify individual structures and to measure their signal intensities accurately from the suboptimal images and ADC maps. In a DWI study of lesions located predominantly around airspaces in the paranasal sinuses or larynx, Wang *et al.* [21] reported that 16% of the lesions had severe local distortions owing to susceptibility artefacts resulting in suboptimal ADC maps. The susceptibility artefacts may be reduced by acquisition of DWI with parallel imaging, performed with a sensitivity encoding (SENSE) factor of 2, which reduces the echo train length, which in turn allows for further reduction of both repetition time and TE and thus, reduces susceptibility artefacts [108,109]. Newer techniques, which are inherently insensitive to artefacts, such as split acquisition of fast spin-echo signals (SPLICE) [110], DWI with line scan data acquisition (LSDWI) [28] and fast asymmetric SE (FASE) [111], have also been recently proposed for acquisition of DWI data. However, very few studies have assessed the usefulness of these techniques in the head and neck region. In a study by Maeda *et al.* [28], the use of LSDWI in distinguishing SCCs from lymphomas of the head and neck was explored. The authors of this study did not observe a problem in evaluating the lesions owing to susceptibility artefacts in any of the cases.

In a DWI study of salivary gland lesions, Yoshino *et al.* [110] reported that better quality DWI images could be obtained using the SPLICE technique compared with the single shot EPI readout strategy. Another study supported the use of SPLICE in obtaining high quality DWI images and reliable ADC values of head and neck mass lesions [112].

Along with the above-mentioned artefacts, motion artefacts also often degrade image quality in clinical scans. Instead of acquiring parallel lines of k-space, as in Cartesian k-space sampling, a modified radial acquisition scheme with rotating parallel lines is proposed [42,113], where each acquired segment represents a single rectilinear blade of a propeller-shaped k-space trajectory [114]. This approach, commonly known as PROPELLER, or BLADE (Siemens AG, Medical Solutions, Erlangen, Germany), inherently oversamples the k-space center and can be used to correct for in-plane motion. BLADE is the product name of a Siemens motion-insensitive FSE sequence, which uses the PROPELLER k-space trajectory. DWI-BLADE sequence provides a better image quality of the head and neck region since it is also insensitive to susceptibility artefacts and hemorrhage and offers better conspicuity for lesions located at the air–tissue interface. However, a drawback of the DWI–BLADE technique compared with the DWI-EPI method is that DWI–BLADE requires a longer acquisition time. Reduced signal:noise ratio is another potential pitfall associated with the DWI-BLADE sequence that can be prevailed over by using a 32-channel coil with an increased integrated parallel acquisition technique factor [115].

Conclusion

Previous studies have demonstrated that DWI is a very promising technique for assessing head and neck cancers. In comparison to contrast-enhanced CT, MRI or FDG-PET studies, DWI

does not require administration of a contrast agent and thus, is completely noninvasive. The DWI data is acquired with a relatively short acquisition time and data processing tools required to compute ADC maps are generally available on clinical scanners. Thus, the DWI sequence can be easily implemented in routine clinical protocol for head and neck MRI. The quantitative nature of ADC values allows for the comparison of results across different centers. Availability of faster imaging sequences, with reduced susceptibility and motion artefacts, will further assist in establishing DWI as a non-invasive biomarker for assessing and monitoring therapeutic response in head and neck cancer. It is worthwhile mentioning that while assessing DWI of head and neck cancers, care must be taken since there may be some overlap between benign and malignant tumors, particularly among the salivary gland tumors. DWI alone may not be adequate for studying head and neck cancers and combining information provided by structural MRI sequences may be more reliable.

Future perspective

In spite of favorable results, clinical application of DWI in the head and neck region has been limited, mainly owing to inherent drawbacks, including susceptibility artefacts and chemical shift artefacts associated with single shot EPI, the most commonly used readout strategy for acquiring the DWI data. However, newer techniques, such as SPLICE, line scan DWI, fast asymmetric spin echo and BLADE (PROPELLER), are being introduced in order to acquire better quality DWI data. These techniques are feasible in clinical settings and provide distortion-free images and ADC maps.

Introduction of several innovative readout strategies will provide better quality DWI images and ADC maps from the head and neck region that have so far been limited by susceptibility and chemical shift artefacts.

Availability of superior and distortion-free DWI images and ADC maps will have strong implications in detecting tumors within the complex anatomical tissues and structures of the head and neck region with improved conspicuity.

Better image quality will improve the accuracy, sensitivity and specificity of DWI in the characterization and differential diagnosis of head and neck cancers. DWI will also provide useful information for differential diagnosis at anatomical locations where a biopsy is difficult to obtain.

Diffusion-weighted imaging will be very helpful in the localization of small-sized lymph nodes, which is critical for determining prognosis and the risk of developing distant metastasis, as well as planning treatment strategies. Moreover, introduction of whole-body DWI holds promise in the detection of local, as well as distant, metastasis in the same setting.

Pretreatment ADC values have the potential to become a prognostic imaging marker for prospectively identifying patients requiring more aggressive treatment approaches.

An inverse correlation between ADC and microvessel density might make ADC a putative marker for detecting angiogenesis in head and neck cancers. It may be hypothesized that increased angiogenesis will result in increased blood flow to the tumor site, which in turn will make the tumor environment suitable for cellular growth by the enhanced delivery of nutrients and oxygen, which will lead to increased cell density and a reduction in ADC of the tumor.

Future multicentric clinical trials using a standardized DWI protocol will provide accurate and reproducible data that is capable of enhancing decision making in the drug developmental process. It is expected that DWI will be able to detect early changes in the cellular environment of a tumor as a result of cytotoxic chemotherapeutic drugs.

Executive summary

Basic principles of diffusion-weighted imaging

- Diffusion-weighted imaging (DWI) is sensitive to thermally-driven molecular water motion, which is impeded by hypercellularity, cell membranes, intracellular organelles and macromolecules present within the tissues.
- The most common approach for the acquisition of DWI data is to use echo-planar imaging-based spin-echo pulse sequences, in which rectangular gradient pulses are applied before and after the 180° refocusing pulse.
- The sensitivity of DWI to diffusion can be altered by varying the diffusion weighting or 'b' values that depend upon the gradient amplitude, the time for which the diffusion gradients are applied and the time interval between diffusion gradients.
- DWI provides useful information for the characterization and differential diagnosis of various head and neck lesions.

Diffusion-weighted imaging in the characterization of head & neck tumors

- DWI has been used to discriminate carcinomas from lymphomas, benign from malignant tumors and necrosis from abscesses of the head and neck region.
- In general, malignant tumors have lower apparent diffusion coefficient (ADC) values compared with benign tumors.
- DWI provides insight into the characterization and staging of lymph nodes in the head and neck region.

Diffusion-weighted imaging in differentiation between viable & necrotic parts of malignant tumors

- ADC maps help in selecting the best biopsy site and in detecting tumor viability in post-treatment follow-up after radiation therapy.

Diffusion-weighted imaging in the prediction & monitoring of early treatment response

- DWI is a promising technique for differentiating residual or recurrent head and neck tumors from postoperative or postradiation changes.
- ADC may be used as an effective early biomarker of treatment outcome and may allow oncologists to change treatment strategies in cases when a subject does not respond to the initial therapy regimen.
- ▪ Successful treatment is generally reflected by an increase in ADC values.

Conclusion

- ▪ DWI could be included in the routine clinical imaging protocol to evaluate head and neck cancers. However, It is also emphasized that DWI alone cannot be reliably used for diagnosis and prognosis estimations of head and neck cancers. DWI provides useful complementary information for conventional structural MRI techniques.

Bibliography

Papers of special note have been highlighted as:

▪ of interest

▪▪ of considerable interest

1. Parkin DM, Bray F, Ferlay J, Pisani P. Global cancer statistics, 2002. CA Cancer J Clin 2005;55:74–108. [PubMed: 15761078]
2. Pande P, Soni S, Kaur J, et al. Prognostic factors in betel and tobacco related oral cancer. Oral Oncol 2002;38:491–499. [PubMed: 12110345]
3. Argiris A, Haraf DJ, Kies MS, Vokes EE. Intensive concurrent chemoradiotherapy for head and neck cancer with 5-fluorouracil- and hydroxyurea-based regimens: reversing a pattern of failure. Oncologist 2003;8:350–360. [PubMed: 12897332]
4. Funk GF, Karnell LH, Robinson RA, et al. Presentation, treatment, and outcome of oral cavity cancer: a national cancer data base report. Head Neck 2002;24:165–180. [PubMed: 11891947]
5. Syrjanen S. Human papillomavirus infections and oral tumors. Med Microbiol Immunol 2003;192:123–128. [PubMed: 12920585]
6. Scully C, Field JK, Tanzawa H. Genetic aberrations in oral or head and neck squamous cell carcinoma (SCCHN): 1. Carcinogen metabolism, DNA repair and cell cycle control. Oral Oncol 2000;36:256–263. [PubMed: 10793327]
7. McGurk M, Chan C, Jones J, O'Regan E, Sherriff M. Delay in diagnosis and its effect on outcome in head and neck cancer. Br J Oral Maxillofac Surg 2005;43:281–284. [PubMed: 15993279]
8. Schechter NR, Gillenwater AM, Byers RM, et al. Can positron emission tomography improve the quality of care for head-and-neck cancer patients? Int J Radiat Oncol Biol Phys 2001;51:4–9. [PubMed: 11516844]
9. Schwartz DL, Rajendran J, Yueh B, et al. Staging of head and neck squamous cell cancer with extended-field FDG-PET. Arch Otolaryngol Head Neck Surg 2003;129:1173–1178. [PubMed: 14623746]
10. Pentenero M, Cistaro A, Brusa M, et al. Accuracy of ^{18}F-FDG-PET/CT for staging of oral squamous cell carcinoma. Head Neck 2008;30:1488–1496. [PubMed: 18767178]
11. Yao M, Smith RB, Graham MM, et al. The role of FDG PET in management of neck metastasis from head-and-neck cancer after definitive radiation treatment. Int J Radiat Oncol Biol Phys 2005;63:991–999. [PubMed: 16099601]
12. McCollum AD, Burrell SC, Haddad RI, et al. Positron emission tomography with ^{18}F-fluorodeoxyglucose to predict pathologic response after induction chemotherapy and definitive chemoradiotherapy in head and neck cancer. Head Neck 2004;26:890–896. [PubMed: 15390197]
13. Imaizumi A, Yoshino N, Yamada I, et al. A potential pitfall of MR imaging for assessing mandibular invasion of squamous cell carcinoma in the oral cavity. AJNR Am J Neuroradiol 2006;27:114–122. [PubMed: 16418368]
14. Ahmad A, Branstetter BFT. CT versus MR: still a tough decision. Otolaryngol Clin North Am 2008;41:1–22. [PubMed: 18261524]
15. Tartaglino LM, Rao VM, Markiewicz DA. Imaging of radiation changes in the head and neck. Semin Roentgenol 1994;29:81–91. [PubMed: 8128271]
16. Mukherji SK, Schiro S, Castillo M, Kwock L, Muller KE, Blackstock W. Proton MR spectroscopy of squamous cell carcinoma of the extracranial head and neck: *in vitro* and *in vivo* studies. AJNR Am J Neuroradiol 1997;18:1057–1072. [PubMed: 9194433]
17. Star-Lack JM, Adalsteinsson E, Adam MF, et al. *In vivo*1h MR spectroscopy of human head and neck lymph node metastasis and comparison with oxygen tension measurements. AJNR Am J Neuroradiol 2000;21:183–193. [PubMed: 10669248]
18. Maldonado X, Alonso J, Giralt J, et al. 31 phosphorus magnetic resonance spectroscopy in the assessment of head and neck tumors. Int J Radiat Oncol Biol Phys 1998;40:309–312. [PubMed: 9457814]
19. Shukla-Dave A, Poptani H, Loevner LA, et al. Prediction of treatment response of head and neck cancers with P-31 MR spectroscopy from pretreatment relative phosphomonoester levels. Acad Radiol 2002;9:688–694. [PubMed: 12061743]

20. Hoskin PJ, Saunders MI, Goodchild K, et al. Dynamic contrast enhanced magnetic resonance scanning as a predictor of response to accelerated radiotherapy for advanced head and neck cancer. Br J Radiol 1999;72:1093–1098. [PubMed: 10700827]

21. Wang J, Takashima S, Takayama F, et al. Head and neck lesions: characterization with diffusion-weighted echo-planar MR imaging. Radiology 2001;220:621–630. [PubMed: 11526259]

22. Sumi M, Sakihama N, Sumi T, et al. Discrimination of metastatic cervical lymph nodes with diffusion-weighted MR imaging in patients with head and neck cancer. AJNR Am J Neuroradiol 2003;24:1627–1634. [PubMed: 13679283]

23▪. Srinivasan A, Dvorak R, Perni K, Rohrer S, Mukherji SK. Differentiation of benign and malignant pathology in the head and neck using 3T apparent diffusion coefficient values: early experience. AJNR Am J Neuroradiol 2008;29:40–44. [PubMed: 17921228]Demonstrates that diffusion-weighted images (DWI) and apparent diffusion coefficient (ADC) maps can be obtained using clinically higher magnetic field (3T) magnets with optimal quality and that ADC values of benign and malignant neck pathologies are significantly different from each other.

24▪▪. Vandecaveye V, De Keyzer F, Nuyts S, et al. Detection of head and neck squamous cell carcinoma with diffusion weighted MRI after (chemo)radiotherapy: correlation between radiologic and histopathologic findings. Int J Radiat Oncol Biol Phys 2007;67:960–971. [PubMed: 17141979] Outlines the importance of DWI in differentiating persistent or recurrent squamous cell carcinoma of the head and neck from nontumoral tissue changes after chemoradiotherapy. These findings may have a significant impact on patient management.

25▪▪. Vandecaveye V, De Keyzer F, Vander Poorten V, et al. Head and neck squamous cell carcinoma: value of diffusion-weighted mr imaging for nodal staging. Radiology 2009;251:134–146. [PubMed: 19251938]Reports that ADC values are more accurate than conventional turbo spin echo MRI for nodal staging. In addition, the manuscript suggests that ADC maps provide added value in the detection of subcentimeter nodal metastases, which are generally not observed by conventional cross-sectional imaging methods including CT scanning, MRI and PET.

26▪. Abdel Razek AA, Kandeel AY, Soliman N, et al. Role of diffusion-weighted echo-planar MR imaging in differentiation of residual or recurrent head and neck tumors and posttreatment changes. AJNR Am J Neuroradiol 2007;28:1146–1152. [PubMed: 17569975]ADC values were demonstrated to differentiate residual or recurrent head and neck tumors from postoperative or postradiation changes.

27▪. Razek AA, Megahed AS, Denewer A, et al. Role of diffusion-weighted magnetic resonance imaging in differentiation between the viable and necrotic parts of head and neck tumors. Acta Radiol 2008;49:364–370. [PubMed: 18365828]Concludes that ADC is helpful in differentiation between viable and necrotic parts of head and neck tumors. These findings may assist better targeting of biopsy sites for accurate histopathological diagnosis.

28. Maeda M, Kato H, Sakuma H, Maier SE, Takeda K. Usefulness of the apparent diffusion coefficient in line scan diffusion-weighted imaging for distinguishing between squamous cell carcinomas and malignant lymphomas of the head and neck. AJNR Am J Neuroradiol 2005;26:1186–1192. [PubMed: 15891182]

29▪▪. Kim S, Loevner L, Quon H, et al. Diffusion-weighted magnetic resonance imaging for predicting and detecting early response to chemoradiation therapy of squamous cell carcinomas of the head and neck. Clin Cancer Res 2009;15:986–994. [PubMed: 19188170]The prognostic value of pretreatment ADC values in the prediction of early treatment response to chemoradiation therapy of patients with squamous cell carcinoma of the head and neck is reported. Early assessment of treatment response may assist in better selection of alternative treatment strategies.

30▪▪. Padhani AR, Liu G, Mu-Koh D, et al. Diffusion-weighted magnetic resonance imaging as a cancer biomarker: consensus and recommendations. Neoplasia 2009;11:102–125. [PubMed: 19186405] Discusses the current understanding of pathophysiologic basis of DWI as a potential cancer biomarker. It also provides recommendations for measurement, image display and analysis methods for clinical DWI data.

31. Tsuruda JS, Chew WM, Moseley ME, Norman D. Diffusion-weighted MR imaging of the brain: value of differentiating between extraaxial cysts and epidermoid tumors. AJR Am J Roentgenol 1990;155:1059–1065. [PubMed: 2120936]

32. Okamoto K, Ito J, Ishikawa K, Sakai K, Tokiguchi S. Diffusion-weighted echo-planar MR imaging in differential diagnosis of brain tumors and tumor-like conditions. Eur Radiol 2000;10:1342–1350. [PubMed: 10939505]
33. Bammer R, Fazekas F. Diffusion imaging of the human spinal cord and the vertebral column. Top Magn Reson Imaging 2003;14:461–476. [PubMed: 14872166]
34. Vandecaveye V, De Keyzer F, Dymarkowski S. Perfusion- and diffusion-weighted imaging of hepatocellular carcinoma. JBR–BTR 2007;90:492–496. [PubMed: 18376763]
35. Kim S, Naik M, Sigmund E, Taouli B. Diffusion-weighted MR imaging of the kidneys and the urinary tract. Magn Reson Imaging Clin N Am 2008;16:585–596. [PubMed: 18926424]
36. Stejskal EO, Tanner J. Spin diffusion measurements: spin echoes in the presence of a time-dependent field gradient. J Chem Phys 1965;42:288–292.
37. Colagrande S, Belli G, Politi LS, Mannelli L, Pasquinelli F, Villari N. The influence of diffusion- and relaxation-related factors on signal intensity: an introductive guide to magnetic resonance diffusion-weighted imaging studies. J Comput Assist Tomogr 2008;32:463–474. [PubMed: 18520558]
38. Gray L, MacFall J. Overview of diffusion imaging. Magn Reson Imaging Clin N Am 1998;6:125–138. [PubMed: 9449744]
39. Thoeny HC, De Keyzer F. Extracranial applications of diffusion-weighted magnetic resonance imaging. Eur Radiol 2007;17:1385–1393. [PubMed: 17206421]
40. Le Bihan D, Breton E, Lallemand D, Grenier P, Cabanis E, Laval-Jeantet M. MR imaging of intravoxel incoherent motions: application to diffusion and perfusion in neurologic disorders. Radiology 1986;161:401–407. [PubMed: 3763909]
41. Turner R, Le Bihan D, Maier J, Vavrek R, Hedges LK, Pekar J. Echo-planar imaging of intravoxel incoherent motion. Radiology 1990;177:407–414. [PubMed: 2217777]
42. Deng J, Miller FH, Salem R, Omary RA, Larson AC. Multishot diffusion-weighted propeller magnetic resonance imaging of the abdomen. Invest Radiol 2006;41:769–775. [PubMed: 16971801]
43. Friedrich KM, Matzek W, Gentzsch S, Sulzbacher I, Czerny C, Herneth AM. Diffusion-weighted magnetic resonance imaging of head and neck squamous cell carcinomas. Eur J Radiol 2008;68:493–498. [PubMed: 19189427]
44. Srinivasan A, Dvorak R, Rohrer S, Mukherji SK. Initial experience of 3-tesla apparent diffusion coefficient values in characterizing squamous cell carcinomas of the head and neck. Acta Radiol 2008;49:1079–1084. [PubMed: 18785024]
45. Gupta RK, Cloughesy TF, Sinha U, et al. Relationships between choline magnetic resonance spectroscopy, apparent diffusion coefficient and quantitative histopathology in human glioma. J Neurooncol 2000;50:215–226. [PubMed: 11263501]
46. Guo AC, Cummings TJ, Dash RC, Provenzale JM. Lymphomas and high-grade astrocytomas: comparison of water diffusibility and histologic characteristics. Radiology 2002;224:177–183. [PubMed: 12091680]
47. Lyng H, Haraldseth O, Rofstad EK. Measurement of cell density and necrotic fraction in human melanoma xenografts by diffusion weighted magnetic resonance imaging. Magn Reson Med 2000;43:828–836. [PubMed: 10861877]
48. Alvarez-Linera J, Benito-Leon J, Escribano J, Rey G. Predicting the histopathological grade of cerebral gliomas using high b value MR DW imaging at 3-tesla. J Neuroimaging 2008;18:276–281. [PubMed: 18482368]
49. Akter M, Hirai T, Makino K, et al. Diffusion-weighted imaging of primary brain lymphomas: effect of ADC value and signal intensity of T2-weighted imaging. Comput Med Imaging Graph 2008;32:539–543. [PubMed: 18617368]
50. Mishra AM, Gupta RK, Saksena S, et al. Biological correlates of diffusivity in brain abscess. Magn Reson Med 2005;54:878–885. [PubMed: 16155895]
51. Kotsenas AL, Roth TC, Manness WK, Faerber EN. Abnormal diffusion-weighted MRI in medulloblastoma: does it reflect small cell histology? Pediatr Radiol 1999;29:524–526. [PubMed: 10398789]

52. Jakobsen J, Hansen O, Jorgensen KE, Bastholt L. Lymph node metastases from laryngeal and pharyngeal carcinomas – calculation of burden of metastasis and its impact on prognosis. Acta Oncol 1998;37:489–493. [PubMed: 9831380]
53. de Bondt RB, Nelemans PJ, Hofman PA, et al. Detection of lymph node metastases in head and neck cancer: a meta-analysis comparing US, US guided FNAC, CT and MR imaging. Eur J Radiol 2007;64:266–272. [PubMed: 17391885]
54. Sigal R, Vogl T, Casselman J, et al. Lymph node metastases from head and neck squamous cell carcinoma: MR imaging with ultrasmall superparamagnetic iron oxide particles (Sinerem MR) – results of a Phase-III multicenter clinical trial. Eur Radiol 2002;12:1104–1113. [PubMed: 11976854]
55. Mack MG, Balzer JO, Straub R, Eichler K, Vogl TJ. Superparamagnetic iron oxide-enhanced MR imaging of head and neck lymph nodes. Radiology 2002;222:239–244. [PubMed: 11756732]
56. White ML, Zhang Y, Robinson RA. Evaluating tumors and tumor like lesions of the nasal cavity, the paranasal sinuses, and the adjacent skull base with diffusion-weighted MRI. J Comput Assist Tomogr 2006;30:490–495. [PubMed: 16778627]
57. Chong VF, Fan YF, Khoo JB. MRI features of cervical nodal necrosis in metastatic disease. Clin Radiol 1996;51:103–109. [PubMed: 8631161]
58. Abdel Razek AA, Soliman NY, Elkhamary S, Alsharaway MK, Tawfik A. Role of diffusion-weighted MR imaging in cervical lymphadenopathy. Eur Radiol 2006;16:1468–1477. [PubMed: 16557366]
59. Koc O, Paksoy Y, Erayman I, Kivrak AS, Arbag H. Role of diffusion weighted MR in the discrimination diagnosis of the cystic and/or necrotic head and neck lesions. Eur J Radiol 2007;62:205–213. [PubMed: 17188444]
60. Saboorian MH, Ashfaq R. The use of fine needle aspiration biopsy in the evaluation of lymphadenopathy. Semin Diagn Pathol 2001;18:110–123. [PubMed: 11403255]
61. Tandon S, Shahab R, Benton JI, Ghosh SK, Sheard J, Jones TM. Fine-needle aspiration cytology in a regional head and neck cancer center: comparison with a systematic review and meta-analysis. Head Neck 2008;30:1246–1252. [PubMed: 18528906]
62. Grunert P, Espinosa J, Busert C, et al. Stereotactic biopsies guided by an optical navigation system: technique and clinical experience. Minim Invasive Neurosurg 2002;45:11–15. [PubMed: 11932818]
63. Gupta S, Madoff DC. Image-guided percutaneous needle biopsy in cancer diagnosis and staging. Tech Vasc Interv Radiol 2007;10:88–101. [PubMed: 18070687]
64. Ang KK, Harris J, Garden AS, et al. Concomitant boost radiation plus concurrent cisplatin for advanced head and neck carcinomas: radiation therapy oncology group Phase II trial 99–14. J Clin Oncol 2005;23:3008–3015. [PubMed: 15860857]
65. Lorch JH, Posner MR, Wirth LJ, Haddad RI. Induction chemotherapy in locally advanced head and neck cancer: a new standard of care? Hematol Oncol Clin North Am 2008;22:1155–1163. [PubMed: 19010265]
66. Mehra R, Cohen RB, Burtness BA. The role of cetuximab for the treatment of squamous cell carcinoma of the head and neck. Clin Adv Hematol Oncol 2008;6:742–750. [PubMed: 18997665]
67. Fajardo LF. Basic mechanisms and general morphology of radiation injury. Semin Roentgenol 1993;28:297–302. [PubMed: 8272878]
68. Lapela M, Grenman R, Kurki T, et al. Head and neck cancer: detection of recurrence with PET and 2-[F-18]fluoro-2-deoxy-D-glucose. Radiology 1995;197:205–211. [PubMed: 7568825]
69. Paulus P, Sambon A, Vivegnis D, et al. ^{18}FDG-PET for the assessment of primary head and neck tumors: clinical, computed tomography, and histopathological correlation in 38 patients. Laryngoscope 1998;108:1578–1583. [PubMed: 9778305]
70. McGuirt WF, Greven KM, Keyes JW Jr, et al. Positron emission tomography in the evaluation of laryngeal carcinoma. Ann Otol Rhinol Laryngol 1995;104:274–278. [PubMed: 7717616]
71. Myers EN, Fagan JJ. Treatment of the N^+ neck in squamous cell carcinoma of the upper aerodigestive tract. Otolaryngol Clin North Am 1998;31:671–686. [PubMed: 9687328]
72. Terhaard CH, Bongers V, van Rijk PP, Hordijk GJ. F-18-fluoro-deoxy-glucose positron-emission tomography scanning in detection of local recurrence after radiotherapy for laryngeal/pharyngeal cancer. Head Neck 2001;23:933–941. [PubMed: 11754496]

73. Hein PA, Eskey CJ, Dunn JF, Hug EB. Diffusion-weighted imaging in the follow-up of treated high-grade gliomas: tumor recurrence versus radiation injury. AJNR Am J Neuroradiol 2004;25:201–209. [PubMed: 14970018]
74. Baur A, Huber A, Arbogast S, et al. Diffusion-weighted imaging of tumor recurrencies and posttherapeutical soft-tissue changes in humans. Eur Radiol 2001;11:828–833. [PubMed: 11372617]
75. Philippens ME, Gambarota G, van der Kogel AJ, Heerschap A. Radiation effects in the rat spinal cord: evaluation with apparent diffusion coefficient versus T2 at serial MR imaging. Radiology 2009;250:387–397. [PubMed: 19037019]
76. Hackney DB. Forget the diffusion – do we need T2-weighted MR images to detect early central nervous system injury? Radiology 2009;250:303–304. [PubMed: 19188306]
77. Zorat PL, Paccagnella A, Cavaniglia G, et al. Randomized Phase III trial of neoadjuvant chemotherapy in head and neck cancer: 10-year follow-up. J Natl Cancer Inst 2004;96:1714–1717. [PubMed: 15547184]
78. Bonner JA, Harari PM, Giralt J, et al. Radiotherapy plus cetuximab for squamous-cell carcinoma of the head and neck. N Engl J Med 2006;354:567–578. [PubMed: 16467544]
79. Chenevert TL, McKeever PE, Ross BD. Monitoring early response of experimental brain tumors to therapy using diffusion magnetic resonance imaging. Clin Cancer Res 1997;3:1457–1466. [PubMed: 9815831]
80. Poptani H, Puumalainen AM, Grohn OH, et al. Monitoring thymidine kinase and ganciclovir-induced changes in rat malignant glioma *in vivo* by nuclear magnetic resonance imaging. Cancer Gene Ther 1998;5:101–109. [PubMed: 9570301]
81. Lemaire L, Howe FA, Rodrigues LM, Griffiths JR. Assessment of induced rat mammary tumour response to chemotherapy using the apparent diffusion coefficient of tissue water as determined by diffusion-weighted 1H-NMR spectroscopy *in vivo*. MAGMA 1999;8:20–26. [PubMed: 10383089]
82. Mardor Y, Roth Y, Ochershvilli A, et al. Pretreatment prediction of brain tumors' response to radiation therapy using high b-value diffusion-weighted MRI. Neoplasia 2004;6:136–142. [PubMed: 15140402]
83. Dzik-Jurasz A, Domenig C, George M, et al. Diffusion MRI for prediction of response of rectal cancer to chemoradiation. Lancet 2002;360:307–308. [PubMed: 12147376]
84. McVeigh PZ, Syed AM, Milosevic M, Fyles A, Haider MA. Diffusion-weighted MRI in cervical cancer. Eur Radiol 2008;18:1058–1064. [PubMed: 18193428]
85. Hermans R, Meijerink M, van den Bogaert W, et al. Tumor perfusion rate determined noninvasively by dynamic computed tomography predicts outcome in head-and-neck cancer after radiotherapy. Int J Radiat Oncol Biol Phys 2003;57:1351–1356. [PubMed: 14630273]
86. Schmitt P, Kotas M, Tobermann A, Haase A, Flentje M. Quantitative tissue perfusion measurements in head and neck carcinoma patients before and during radiation therapy with a non-invasive MR imaging spin-labeling technique. Radiother Oncol 2003;67:27–34. [PubMed: 12758237]
87. Robinson SP, Collingridge DR, Howe FA, et al. Tumour response to hypercapnia and hyperoxia monitored by flood magnetic resonance imaging. NMR Biomed 1999;12:98–106. [PubMed: 10392806]
88. Gandhi D, Chepeha DB, Miller T, et al. Correlation between initial and early follow-up CT perfusion parameters with endoscopic tumor response in patients with advanced squamous cell carcinomas of the oropharynx treated with organ-preservation therapy. AJNR Am J Neuroradiol 2006;27:101–106. [PubMed: 16418366]
89. Cao Y, Popovtzer A, Li D, et al. Early prediction of outcome in advanced head-and-neck cancer based on tumor blood volume alterations during therapy: a prospective study. Int J Radiat Oncol Biol Phys 2008;72:1287–1290. [PubMed: 19028268]
90. Zima A, Carlos R, Gandhi D, et al. Can pretreatment CT perfusion predict response of advanced squamous cell carcinoma of the upper aerodigestive tract treated with induction chemotherapy? AJNR Am J Neuroradiol 2007;28:328–334. [PubMed: 17297007]
91. Kauppinen RA. Monitoring cytotoxic tumour treatment response by diffusion magnetic resonance imaging and proton spectroscopy. NMR Biomed 2002;15:6–17. [PubMed: 11840548]
92. Heller KS, Attie JN. Treatment of warthin's tumor by enucleation. Am J Surg 1988;156:294–296. [PubMed: 3177754]

93. Witt RL. The significance of the margin in parotid surgery for pleomorphic adenoma. Laryngoscope 2002;112:2141–2154. [PubMed: 12461331]
94. Al-Khafaji BM, Nestok BR, Katz RL. Fine-needle aspiration of 154 parotid masses with histologic correlation: ten-year experience at the University of Texas M D Anderson Cancer Center. Cancer 1998;84:153–159. [PubMed: 9678729]
95. Zbaren P, Nuyens M, Loosli H, Stauffer E. Diagnostic accuracy of fine-needle aspiration cytology and frozen section in primary parotid carcinoma. Cancer 2004;100:1876–1883. [PubMed: 15112268]
96. Mukunyadzi P, Bardales RH, Palmer HE, Stanley MW. Tissue effects of salivary gland fine-needle aspiration Does this procedure preclude accurate histologic diagnosis? Am J Clin Pathol 2000;114:741–745. [PubMed: 11068548]
97. Mighell AJ, High AS. Histological identification of carcinoma in 21 gauge needle tracks after fine needle aspiration biopsy of head and neck carcinoma. J Clin Pathol 1998;51:241–243. [PubMed: 9659269]
98. Freling NJ, Molenaar WM, Vermey A, et al. Malignant parotid tumors: clinical use of MR imaging and histologic correlation. Radiology 1992;185:691–696. [PubMed: 1438746]
99. Joe VQ, Westesson PL. Tumors of the parotid gland: MR imaging characteristics of various histologic types. AJR Am J Roentgenol 1994;163:433–438. [PubMed: 8037045]
100. Habermann CR, Gossrau P, Graessner J, et al. Diffusion-weighted echo-planar MRI: a valuable tool for differentiating primary parotid gland tumors? Rofo 2005;177:940–945. [PubMed: 15973595]
101. Eida S, Sumi M, Sakihama N, Takahashi H, Nakamura T. Apparent diffusion coefficient mapping of salivary gland tumors: prediction of the benignancy and malignancy. AJNR Am J Neuroradiol 2007;28:116–121. [PubMed: 17213436]
102. Yabuuchi H, Matsuo Y, Kamitani T, et al. Parotid gland tumors: can addition of diffusion-weighted MR imaging to dynamic contrast-enhanced MR imaging improve diagnostic accuracy in characterization? Radiology 2008;249:909–916. [PubMed: 18941162]
103. Habermann CR, Arndt C, Graessner J, et al. Diffusion-weighted echo-planar MR imaging of primary parotid gland tumors: is a prediction of different histologic subtypes possible? AJNR Am J Neuroradiol 2009;30:591–596. [PubMed: 19131405]
104. Matsushima N, Maeda M, Takamura M, Takeda K. Apparent diffusion coefficients of benign and malignant salivary gland tumors. Comparison to histopathological findings. J Neuroradiol 2007;34:183–189. [PubMed: 17568674]
105. Vogl TJ, Dresel SH, Spath M, et al. Parotid gland: plain and gadolinium-enhanced MR imaging. Radiology 1990;177:667–674. [PubMed: 2243966]
106. Huisman TA, Loenneker T, Barta G, et al. Quantitative diffusion tensor MR imaging of the brain: field strength related variance of apparent diffusion coefficient (ADC) and fractional anisotropy (FA) scalars. Eur Radiol 2006;16:1651–1658. [PubMed: 16532356]
107. Grieve SM, Blamire AM, Styles P. Elimination of nyquist ghosting caused by read-out to phase-encode gradient cross-terms in EPI. Magn Reson Med 2002;47:337–343. [PubMed: 11810678]
108. Schmitz BL, Aschoff AJ, Hoffmann MH, Gron G. Advantages and pitfalls in 3T MR brain imaging: a pictorial review. AJNR Am J Neuroradiol 2005;26:2229–2237. [PubMed: 16219827]
109. Bammer R, Schoenberg SO. Current concepts and advances in clinical parallel magnetic resonance imaging. Top Magn Reson Imaging 2004;15:129–158. [PubMed: 15479997]
110. Yoshino N, Yamada I, Ohbayashi N, et al. Salivary glands and lesions: evaluation of apparent diffusion coefficients with split-echo diffusion-weighted MR imaging – initial results. Radiology 2001;221:837–842. [PubMed: 11719687]
111. Kito S, Morimoto Y, Tanaka T, et al. Utility of diffusion-weighted images using fast asymmetric spin-echo sequences for detection of abscess formation in the head and neck region. Oral Surg Oral Med Oral Pathol Oral Radiol Endod 2006;101:231–238. [PubMed: 16448927]
112. Sakamoto J, Yoshino N, Okochi K, et al. Tissue characterization of head and neck lesions using diffusion-weighted MR imaging with SPLICE. Eur J Radiol 2009;69:260–268. [PubMed: 18023549]
113. Wintersperger BJ, Runge VM, Biswas J, et al. Brain magnetic resonance imaging at 3 tesla using BLADE compared with standard rectilinear data sampling. Invest Radiol 2006;41:586–592. [PubMed: 16772852]

114. Pipe JG. Motion correction with PROPELLER MRI: application to head motion and free-breathing cardiac imaging. Magn Reson Med 1999;42:963–969. [PubMed: 10542356]

115. Fries P, Runge VM, Kirchin MA, et al. Diffusion-weighted imaging in patients with acute brain ischemia at 3 T: current possibilities and future perspectives comparing conventional echoplanar diffusion-weighted imaging and fast spin echo diffusion-weighted imaging sequences using BLADE (PROPELLER). Invest Radiol 2009;44:351–359. [PubMed: 19363447]

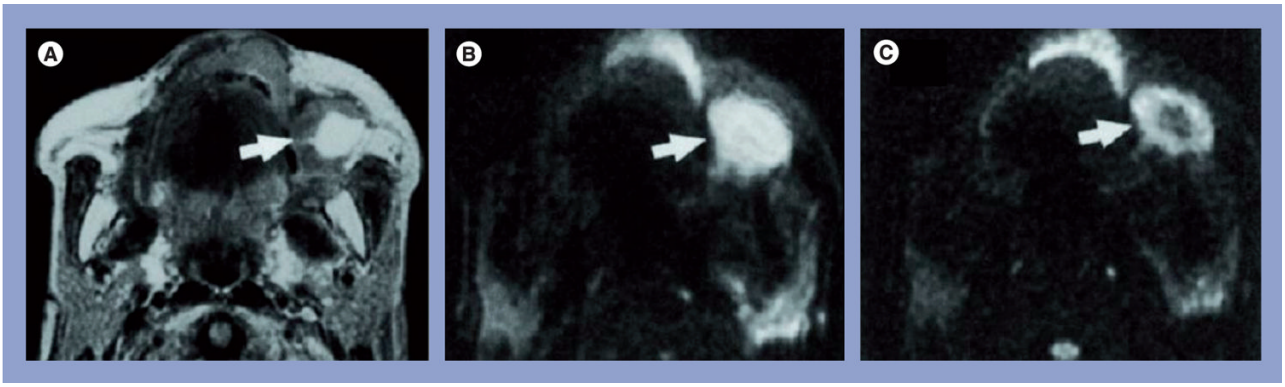

Figure 1. Representative case of a well-differentiated squamous cell carcinoma of the maxilla
(A) Axial spin–spin relaxation time-weighted image of a metastatic buccinator node (arrow) that shows a large, hyperintense necrotic area. **(B)** Axial diffusion-weighted echo-planar MR image at b factor of 500 s/mm^2, the metastatic node appears hyperintense (arrow). **(C)** Axial diffusion-weighted echo-planar MR image at b factor of 1000 s/mm^2, the metastatic node exhibits a central hypointense area (arrow) corresponding to the partially necrotic portion of the node. The mean apparent diffusion coefficient of the node was 0.410×10^{-3} mm^2/s.
MR: Magnetic resonance.
Reprinted with permission from [22].

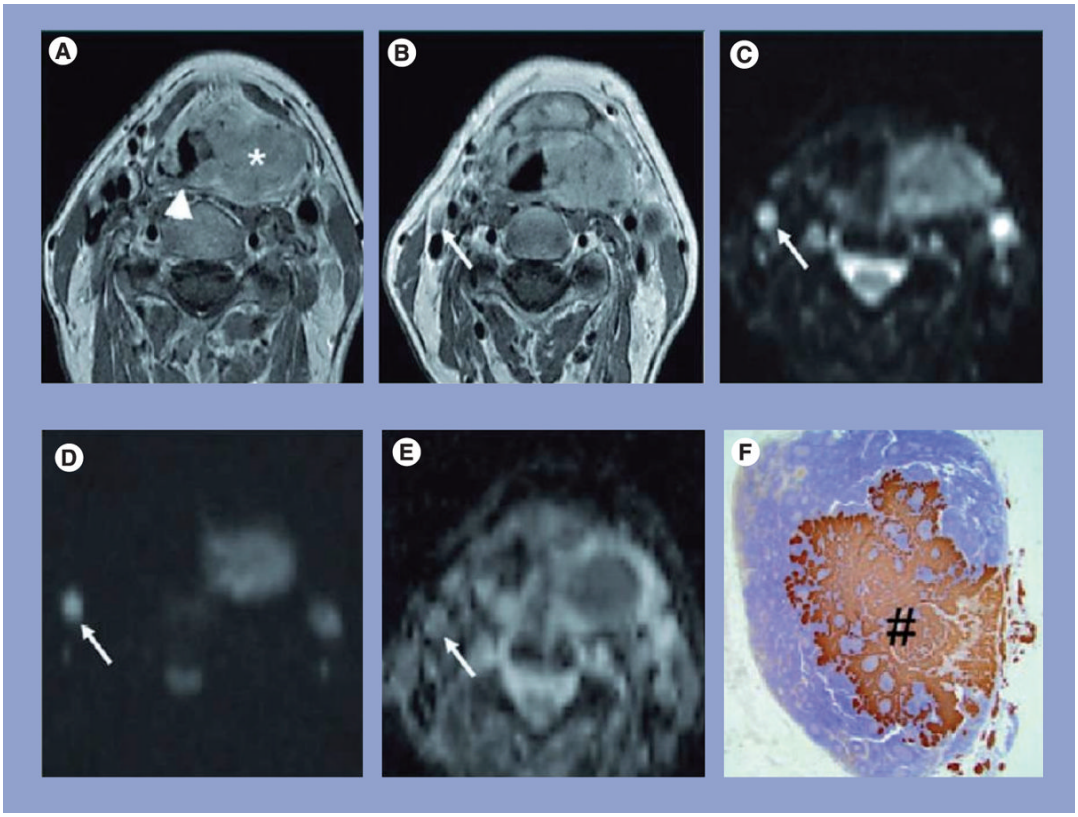

Figure 2. Representative MRI and pathology sections of a squamous cell carcinoma patient with metastatic lymph node

(A) Transverse gadolinium-enhanced T1-weighted TSE MR image in a 57-year-old man shows a large left-sided tumor mass (*) centered on the piriform sinus involving the supraglottic gland and crossing the midline on the posterior pharyngeal wall (arrowhead). **(B)** Transverse gadolinium-enhanced T1-weighted TSE MR image from the same patient shows a small oval-shaped lymph node at level 2 on the right side with a shortest transverse diameter of 0.6 cm (arrow); this lymph node was considered to be negative for cancer. **(C)** The lymph node (arrow) is hyperintense on the b = 0 s/mm^2 image. **(D)** Only a limited signal loss is seen on the b = 1000 s/mm^2 DWI image. **(E)** The ADC map demonstrated the lymph node to have an ADC value of 0.71×10^{-3} mm^2/s, which was suspicious for metastatic adenopathy. **(F)** Corresponding prekeratin-stained histopathologic slice shows an intranodal metastatic deposit (#).

ADC: Apparent diffusion coefficient; T1: Spin-lattice relaxation; TSE MR: Turbo spin-echo magnetic resonance.

Reprinted with permission from [25].

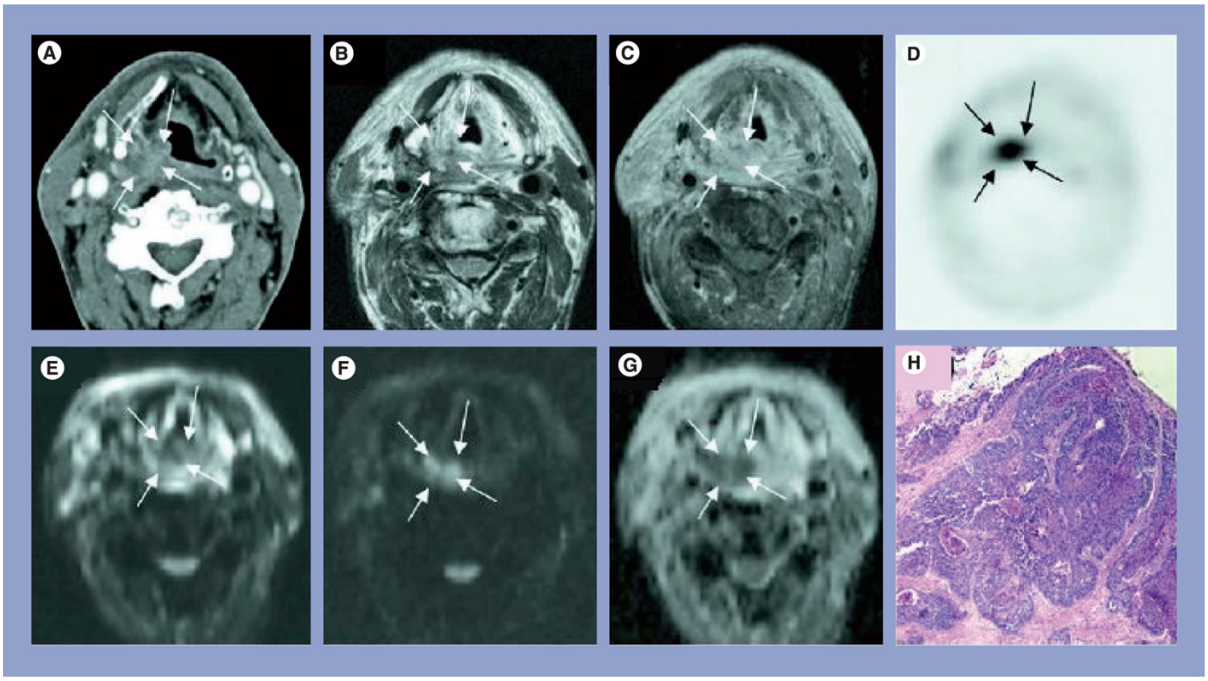

Figure 3. Representative MRI and pathology sections from a squamous cell carcinoma patient who demonstrated recurrences at the local site

(A) Computed tomography image showing asymmetric soft tissue thickening in the right aryepiglottic fold and piriform sinus that is suspected for tumor recurrence (arrows). **(B)** Spin–spin relaxation time-weighted turbo spin-echo image, and **(C)** post-contrast T1-weighted TSE image confirm the presence of the right hypopharyngeal mass. **(D)** The lesion correlates with focal increased tracer-uptake on the 18-fluorodeoxyglucose positron emission tomography image; **(E)** on diffusion-weighted MRI, the lesion is hypointense compared with the surrounding tissues on the b = 0 s/mm^2 image, **(F)** hyperintense on the b = 1000 s/mm^2 image, and **(G)** hypointense on the apparent diffusion coefficient map, thereby showing restricted diffusion and is indicative of a hypercellular lesion:tumor recurrence. **(H)** Tumor recurrence was confirmed on histopathology.

T1: Spin-lattice relaxation; TSE: Turbo spin echo.

Reprinted with permission from [24].

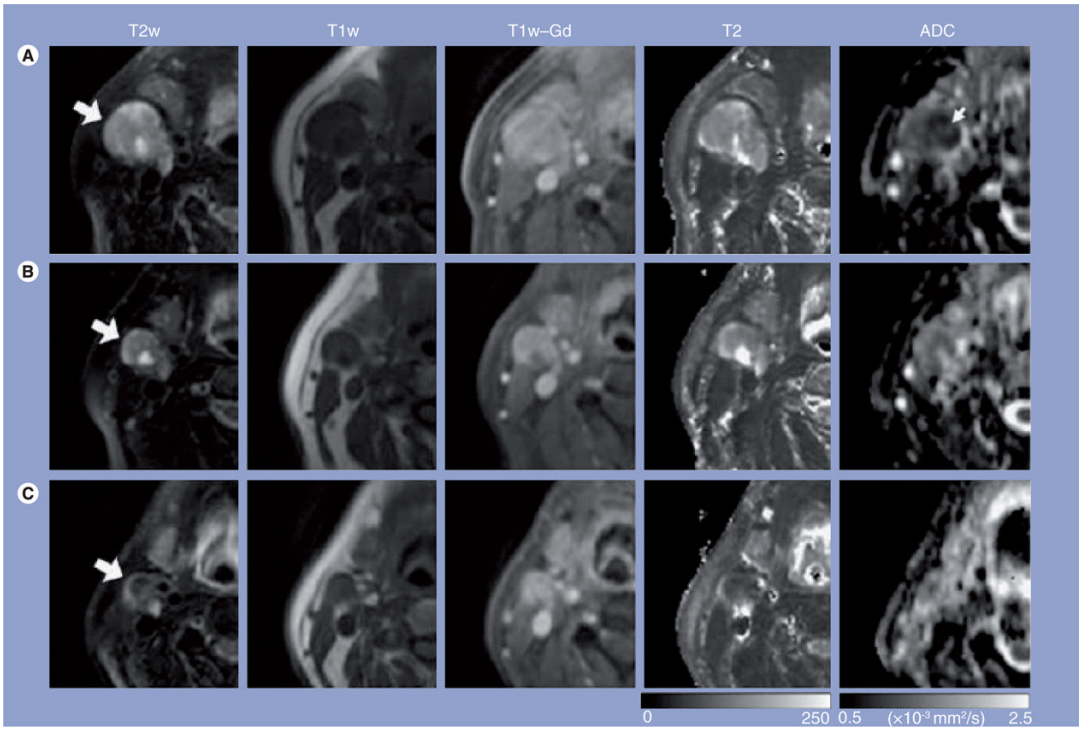

Figure 4. Representative images of a patient who exhibited complete response to treatment

Images in each row are from three measurement time points: **(A)** pretreatment, **(B)** 1 week into chemoradiation therapy and **(C)** post-treatment. The T2w, T1w and T1w-Gd images were windowed to have similar image contrast, whereas spin–spin relaxation time and ADC images were scaled based on the grayscale bars shown at the bottom of the corresponding images. Large arrows point to the same nodal metastatic mass that was followed through the treatment course; the small arrow (ADC map) shows the central region of the mass with lower ADC values than the peripheral region.

ADC: Apparent diffusion coefficient; T1: Spin-lattice relaxation; T2: Spin–spin relaxation time; T1w: T1-weighted; T1w-Gd: T1-weighted postcontrast enhanced; T2w: T2-weighted.

Reprinted with permission from [29].

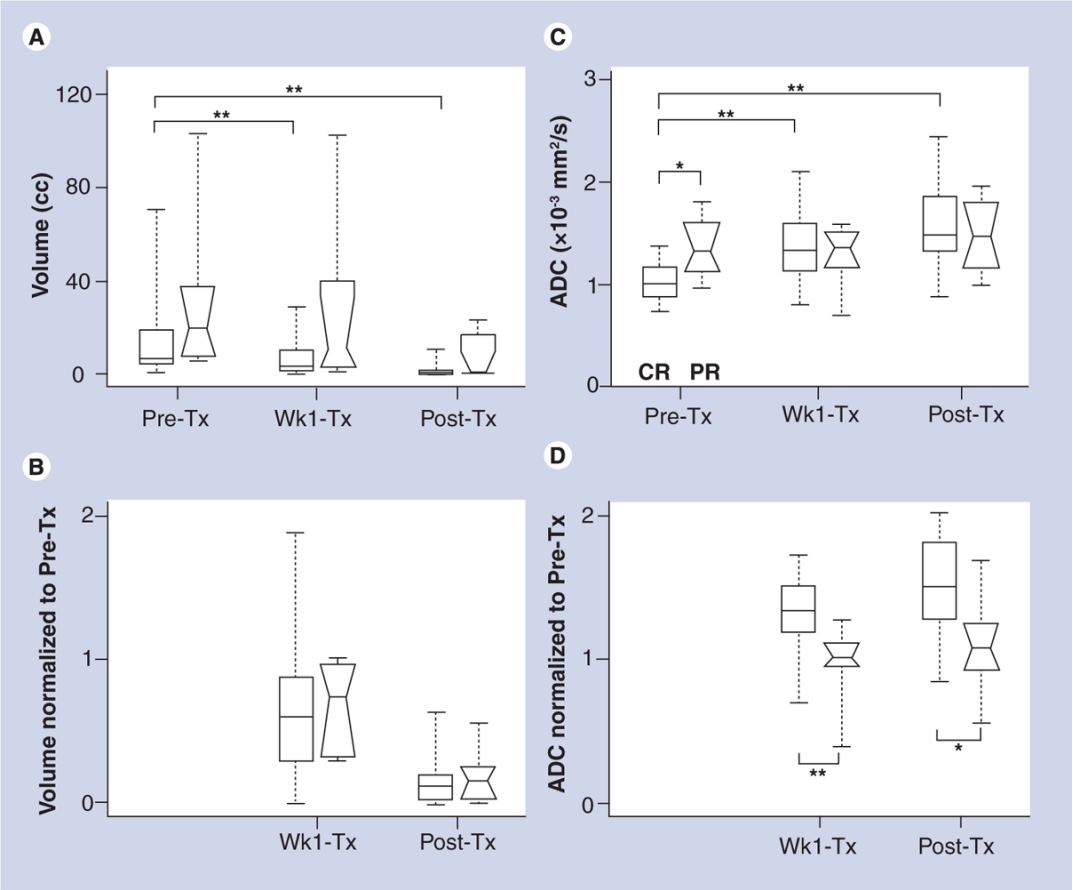

Figure 5. Box and whisker plots from the metastatic node of squamous cell carcinoma patients

Comparison of complete responders (rectangular boxes) and partial responders (boxes with notches) to chemoradiation therapy in terms of **(A)** volume, **(B)** normalized (to pretreatment) volume, **(C)** ADC and **(D)** normalized ADC. Edges of the boxes represent the 25th and 75th percentiles while the middle lines in the boxes show the median values. Whisker lines are the minimum and maximum values.

$^{*}p < 0.05$; $^{**}p < 0.01$.

ADC: Apparent diffusion coefficient; cc: Cubic centimeters; CR: Complete responders; PR: Partial responders; Pre-Tx: Pretreatment; Post-Tx: Post treatment; Wk1-Tx: 1 week into treatment.

Reprinted with permission from [29].